Case Study

Risk Assessment of Earthquake-Triggered Geohazards Surrounding Wenchuan, China

Hai-Min Lyu, Ph.D., S.M.ASCE[1]; Shui-Long Shen, Ph.D., A.M.ASCE[2]; Jun Yang, Ph.D., F.ASCE[3]; and An-Nan Zhou, Ph.D.[4]

Abstract: The great 2008 Wenchuan earthquake in China was a painful disaster. Accordingly, the management and mitigation of the risk of future earthquake-triggered geohazards remain a critical responsibility of local authorities. This case study assesses the risk of earthquake-triggered geohazards surrounding Wenchuan County using the analytical hierarchical process (AHP) and the trapezoidal fuzzy AHP (FAHP). The assessment results show that the regions with high-risk and very high-risk levels are distributed in the belt along the Longmenshan fault zone. Moreover, the percentages of high and very high-risk levels obtained from the trapezoidal FAHP are higher than those obtained from the original AHP. This comparison reveals that the trapezoidal FAHP provides a more reasonable assessment than the AHP. Further, the trapezoidal FAHP can capture the regions with high-risk and very high-risk levels. The results from the trapezoidal FAHP provide four choices that stakeholders can use to make decisions, which mitigates the biases that exist in the original AHP. **DOI: 10.1061/(ASCE)NH.1527-6996.0000375.**

Author keywords: Risk assessment; Wenchuan earthquake; Trapezoidal fuzzy analytical hierarchical process (FAHP); Geographic information system (GIS).

Introduction

The great Wenchuan earthquake of May 12, 2008, was the largest and the most destructive quake that has occurred in China during the past 40 years. This earthquake had a magnitude of M_w 8.0, with its epicenter in Yingxiu Town, Wenchuan County (Sichuan Province, China). This catastrophic earthquake triggered thousands of geohazards, including landslides, debris flows, and slope collapses. According to official records, there were more than 500,000 geohazards triggered by the earthquake, of which 120,000 posed a direct or indirect threat to towns and villages (Qi et al. 2010; Xu et al. 2014; Fan et al. 2018). Earthquake-triggered geohazards are responsible for deaths and economic losses, particularly in mountainous areas, where the damage caused by earthquake-triggered geohazards (e.g., landslides and collapses) can be more severe than the damage caused directly by the earthquake. Accordingly, earthquake-triggered geohazards have attracted worldwide attention (Huang and Li 2014; Lu and Xu 2015).

The Wenchuan earthquake struck the middle segment of the Longmenshan fault belt, which is in the mountainous region of northwest Sichuan Province. The epicenter is characterized by rugged topography, including steep mountains, deep valleys, and complex geological structures. In this complicated geological environment, a large variety of coseismic geohazards were induced. Based on existing research, the Wenchuan earthquake triggered more than 200,000 landslides, resulting in more than 20,000 deaths (Yin et al. 2009; Xu et al. 2014). Most of Beichuan County was destroyed by landslides triggered by the earthquake and aftershocks (Xu et al. 2014; Wang et al. 2014; Fan et al. 2018).

The Wenchuan earthquake has attracted the attention of scientific scholars worldwide. Researchers are focusing on the evolution of geohazards, long-term development of topography, early warning systems, and risk assessments after earthquakes (Zhang and Wang 2007; Wang et al. 2014). Zhou et al. (2016) used a method to identify the potential of debris flow caused by rainfall in the catchments of the Wenchuan earthquake zone. Zhang (2016) assessed household vulnerability and economic impact after the Wenchuan earthquake. Yao and Li (2016) made a space-time assessment of debris flow risk from 2008 to 2013 after the Wenchuan earthquake. However, these studies did not provide any overall plans to manage future risks for Wenchuan County and the surrounding regions.

The analytical hierarchical process (AHP) is a comprehensive risk assessment method based on multicritical indices, which can perform both qualitative and quantitative risk analyses (Saaty 2008, 2010). In AHP, a number from 1 to 9 (or their reciprocals) is assigned to linguistic terms to prioritize the most critical risk assessment factors (Saaty 1977). A judgment matrix is constructed from these assessment factors using these numbers. The AHP method combined with the geographic information system (GIS) has been widely used to assess environmental risks within a region (Godschalk 2003; Kamal et al. 2013; Jalayer et al. 2014; Liu et al. 2016; Gallina et al. 2016).

[1]Postdoctoral Research Associate, Dept. of Civil and Environmental Engineering, College of Engineering, Shantou Univ., Shantou, Guangdong 515063, China. Email: lvhaimin12@163.com

[2]Professor and Dean of College of Engineering, Key Laboratory of Intelligent Manufacturing Technology, Ministry of Education, Shantou Univ., Shantou, Guangdong 515063, China (corresponding author). ORCID: https://orcid.org/0000-0002-5610-7988. Email: shensl@stu.edu.cn

[3]Professor, Dept. of Civil Engineering, Univ. of Hong Kong, Pokfulam, Hong Kong, China; Distinguished Visiting Professor, School of Naval Architecture, Ocean, and Civil Engineering, Shanghai Jiao Tong Univ., Shanghai 200240, China. Email: junyang@hku.hk

[4]Associate Professor, Civil and Infrastructure Engineering Discipline, School of Engineering, Royal Melbourne Institute of Technology, VIC 3001, Australia. Email: annan.zhou@rmit.edu.au

Note. This manuscript was submitted on January 6, 2019; approved on November 6, 2019; published online on May 15, 2020. Discussion period open until October 15, 2020; separate discussions must be submitted for individual papers. This paper is part of the ***Natural Hazards Review***, © ASCE, ISSN 1527-6988.

The AHP method employs a single value to express the judgments of experts. However, an expert's opinion might not be effectively captured using an exact number; instead, providing an interval number may be preferred. To overcome this limitation, an extension to the original AHP has been proposed that uses a fuzzy number to replace an exact number to express the viewpoints of experts (Laarhoven and Pedrycz 1983; Cheng and Mon 1994; Zhang et al. 2015, 2017; Lyu et al. 2019a). The trapezoidal fuzzy number method can arithmetically assign a fuzzy number computed from several variables. Using a trapezoidal fuzzy number to express the judgments of experts is more reasonable than using a crisp number. This study adopts both trapezoidal fuzzy AHP (FAHP) and the original AHP to assess the risk of earthquake-triggered geohazards surrounding Wenchuan County.

The objectives of this study are as follows: (1) assess the risk of earthquake-triggered geohazards surrounding Wenchuan County using the AHP and trapezoidal FAHP methods, and (2) illustrate the efficiency of the trapezoidal FAHP by comparing results from the AHP and trapezoidal FAHP methods.

Materials and Methods

Study Area and Data Sources

The Wenchuan earthquake that occurred in Yingxiu Town was a catastrophe that attracted worldwide attention. According to previous investigations (Huang 2011; Xu et al. 2014), the distribution of geohazards triggered by this earthquake was situated along the Longmenshan fault zone. Therefore, this research focused on the region within the Longmenshan fault belt zone. Fig. 1 shows the location and topography of the study area. The study area covers more than 71,000 km^2, including 29 counties. In the study area, the number of geohazards recorded was more than 100 in each county (Huang 2011; Huang and Li 2014). As shown in Fig. 1, the northwest region is mountainous, whereas the southeast region is flat. The Longmenshan fault zone is located in the transition zone between the mountainous and flat regions. The earthquake epicenter is in the Longmenshan fault zone, which is the seismogenic fault. In this study, the topographic data were extracted using the digital elevation model (DEM) and GDC (2018). The gross domestic product (GDP) data and population density in the study area were obtained from REDCP (2018). Information on the land-use types in the study area was extracted from remote sensory image data.

Assessment Model

Risk is the probability of losses resulting from hazardous events, which is defined as the combination of hazard, exposure, and vulnerability (Lyu et al., forthcoming). A hazard is defined as a potentially destructive natural phenomenon that causes damage and loss to property, infrastructure, service provisions, and environmental resources. Exposure represents factors such as location, and value of assets within a location such as people, buildings, factories, and infrastructures that are exposed to a hazard. Vulnerability refers to the reaction of an asset exposed to the spatial variable forces produced by a hazardous event. The social responses to a hazard event can vary greatly depending on different local socioeconomic conditions. In general, the risk can be described by Eq. (1) as follows:

$$\text{Risk} = \text{Hazard} \otimes \text{Exposure} \otimes \text{Vulnerability} \quad (1)$$

where $\otimes$ is not a simple mathematical symbol—it represents an overlay analysis in the GIS. The quantitative relationship between these three factors can be expressed by the indices of hazard,

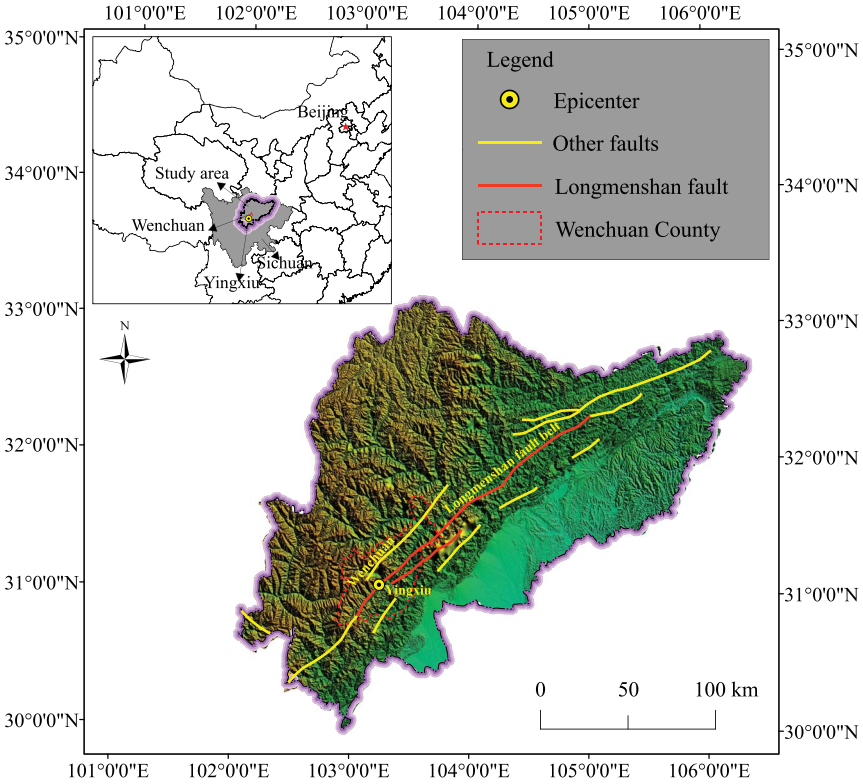

Fig. 1. Location and topography of the study area.

Nat. Hazards Rev., 2020, 21(3): 05020007

exposure, and vulnerability with their corresponding weights. Therefore, the risk is redefined as

$$R = w_H\left(\sum_{i=1}^{n} h_i H_i\right)_{\text{Hazard}} \otimes w_E\left(\sum_{j=1}^{n} e_j E_j\right)_{\text{Exposure}} \otimes w_V\left(\sum_{k=1}^{n} v_k V_k\right)_{\text{Vulnerability}} \quad (2)$$

where w_H, w_E, and w_V = weights of the hazard index, exposure index, and vulnerability index, respectively; h_i, e_j, and v_k = weights of the hazard, exposure, and vulnerability indices, respectively; and H_i, E_j, and V_k = different assessment factors.

Assessment Structure

Fig. 2 provides a flowchart of the assessment procedure for the risk of earthquake-triggered geohazards. As shown in Fig. 2, the assessment structure includes an objective layer, an index layer, and a subindex layer. The objective layer is labeled as (R). The index layer consists of the hazard index (R_1), exposure index (R_2), and vulnerability index (R_3). The subindex layer includes 10 assessment factors, and the determination of each assessment factor is based on the accessibility of data sources.

1. Hazard index (R_1)

   The hazard index is used to reflect the characteristics of the earthquake, which is represented by three subindices: geohazard number (R_{11}), fault density (R_{12}), and fault proximity (R_{13}). The geohazard number is assigned based on field investigations and previous publications (Huang and Li 2014; Xu et al. 2014; Fan et al. 2018). Regions with a large geohazard number have a high risk. Moreover, the distribution of faults has a critical effect on the occurrence of geohazards. Fault density and proximity reflect the influence of a fault. Fault density is the length of a fault per unit area, while fault proximity is the distance to the closest fault.
2. Exposure index (R_2)

   The exposure index represents the characteristics of the disaster-bearing body, including the factors of elevation (R_{21}), slope (R_{22}), river system density (R_{23}), and river system proximity (R_{24}) (Huang 2011; Huang and Li 2014). The elevation and slope were obtained from the DEM in GIS. The procedure of obtaining the river network proximity and density is further discussed in the next section.
3. Vulnerability index (R_3)

   The vulnerability index represents the resistance of the disaster-bearing body, including land-use type (R_{31}), population density (R_{32}), and GDP per unit area (R_{33}) (Huang 2011; Huang and Li 2014). The difference between exposure and vulnerability is that the former is used to reflect the natural features of the study area, while the latter is used to represent the characteristics of related anthropic activities.

Based on the assessment structure, both the AHP and trapezoidal FAHP methods were used to calibrate the assessment factor weights. All assessment factors were normalized before analysis. The normalized factors combined with their corresponding weights were incorporated into the GIS to obtain a spatial distribution of risk levels. The AHP and the trapezoidal FAHP results were then compared.

Weight Calibration

AHP Method

As shown in Eq. (3), the judgment matrix is used to show the relative importance of the assessment factors in the AHP method. In the judgment matrix, x_{ij} is the relative value of the factor i to j, which ranges from 1 to 9, and their reciprocals (Saaty 1977). When x_i is significantly more important than x_j, x_{ij} is equal to 9, and x_{ji} is

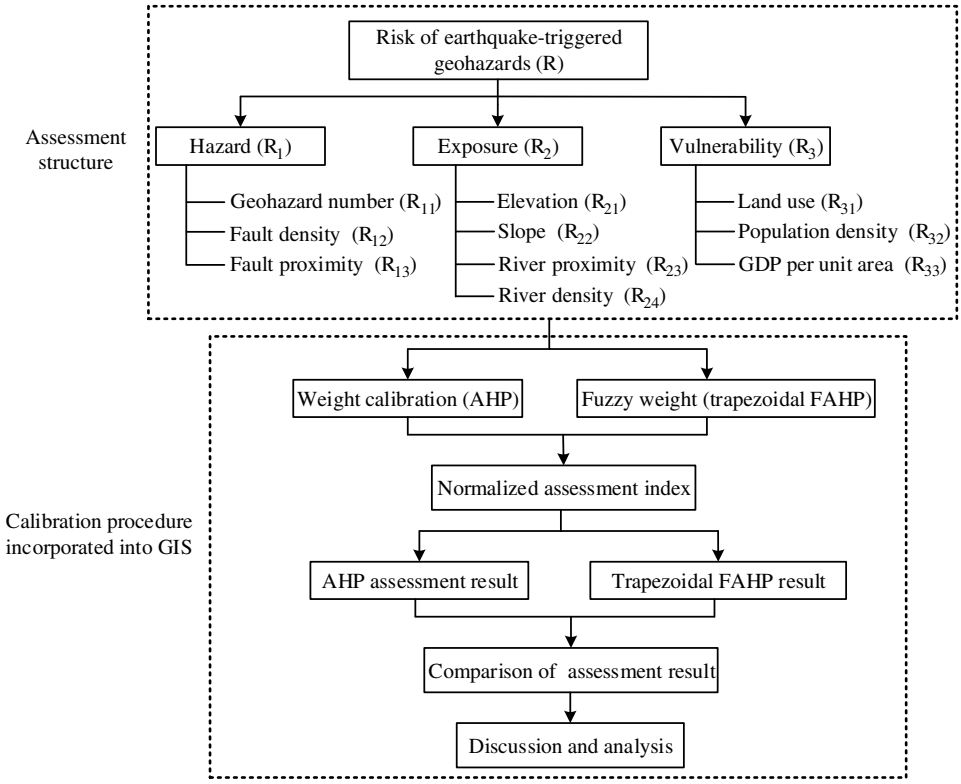

Fig. 2. Flowchart of the assessment procedure for the risk of earthquake-triggered geohazards.

Nat. Hazards Rev., 2020, 21(3): 05020007

equal to 1/9. The weight calibration procedure is the calculation of the corresponding eigenvector using the largest eigenvalue in the judgment matrix

$$\mathbf{X}_u = (x_{ij})_{n\times n} = \begin{pmatrix} 1 & \cdots & x_{1n} \\ \vdots & 1 & \vdots \\ x_{n1} & \cdots & 1 \end{pmatrix} \tag{3}$$

where X_u = judgment matrix. The weights of the assessment factors can be calibrated using Eq. (4)

$$w_i = \frac{M_i}{\sum_{i=1}^{n} M_i} \tag{4}$$

where $M_i = \sqrt[n]{\prod_{j=1}^{n} x_{ij}}$. According to Saaty's research (Saaty 1977), the judgment matrix is consistent if the consistency ratio (CR) is less than 0.1. The value of the CR can be calibrated using Eq. (5)

$$CR = \frac{CI}{RI} \tag{5}$$

where $CI = (\lambda_{\max} - n)/(n-1)$ and $\lambda_{\max}$ = largest eigenvalue in the judgment matrix (X_u), which can be calibrated from Eq. (6); and RI = average random consistency index (Saaty 1977; Lyu et al. 2018a, b; 2019a)

$$\lambda_{\max} = \sum_{i=1}^{n} \frac{\sum_{j=1}^{n} x_{ij} w_i}{n w_i} \tag{6}$$

Trapezoidal FAHP

Once the judgment matrix (X_u) meets the consistency requirement, each element in the judgment matrix is replaced by a trapezoidal fuzzy number. Table 1 lists the linguistic variables of a trapezoidal fuzzy number with a corresponding exact number. Fig. 3 shows the membership of trapezoidal fuzzy numbers. As shown in Fig. 3, when $p_2 = p_3$, P is a triangular fuzzy number; when $p_1 = p_2$ and $p_3 = p_4$, P is an interval number; and when $p_1 = p_2 = p_3 = p_4$, P is a real value (original AHP). Therefore, trapezoidal fuzzy numbers can arithmetically process and intuitively interpret fuzzy numbers in a variable way. This feature of fuzzy numbers is the reason we selected the trapezoidal FAHP method to assess risk. In this research, a trapezoidal fuzzy number is applied to calculate the weights of the assessment factors.

Table 1. Linguistic variables and corresponding trapezoidal fuzzy number

Linguistic terms	Original assignment (AHP)	Trapezoidal fuzzy number
Equal	1	$1' = (1, 1, 1, 1)$
Slightly strong	3	$3' = (1, 1.222, 1.857, 2.333)$
Fairly strong	5	$5' = (1.5, 1.857, 3, 4)$
Very strong	7	$7' = (2.333, 3, 5.667, 9)$
Absolutely strong	9	$9' = (4, 5.667, 9, 9)$

Note: (2, 4, 6, 8) and (2′, 4′, 6′, 8′) indicate the importance degrees that belong to interval variables.

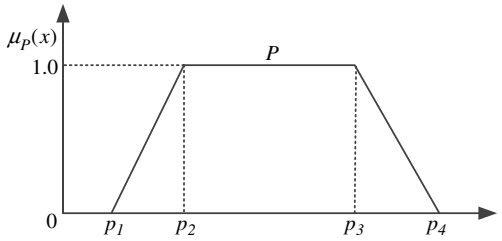

Fig. 3. Membership of a trapezoidal fuzzy number.

Following the value determination within the judgment matrix, an extended judgment matrix $A_u = [P_{ij}]_{n\times n}$ with a trapezoidal fuzzy number is obtained. The fuzzy weight of the extended judgment matrix is calculated using an average geometric method as

$$\vec{w}_j = (w_{j1}, w_{j2}, w_{j3}, w_{j4}) = \left(\frac{p_{1i}}{p_4}, \frac{p_{2i}}{p_3}, \frac{p_{3i}}{p_2}, \frac{p_{4i}}{p_1}\right) \tag{7}$$

where w_{j1}, w_{j2}, w_{j3}, and w_{j4} = fuzzy weights of the trapezoidal fuzzy judgment matrix; and $0 < w_{j1} < w_{j2} < w_{j3} < w_{j4} < 1$, p_{1i}, p_{2i}, p_{3i}, and p_{4i} are the values of the trapezoidal fuzzy judgment matrix $A_u = [P_{ij}]_{n\times n}$, which can be calculated using the following equation:

$$p_{1i} = \left(\prod_{j=1}^{n} p_{2ij}\right)^{1/n}, \quad p_{2i} = \left(\prod_{j=1}^{n} p_{2ij}\right)^{1/n},$$
$$p_{3i} = \left(\prod_{j=1}^{n} p_{3ij}\right)^{1/n}, \quad p_{4i} = \left(\prod_{j=1}^{n} p_{4ij}\right)^{1/n}$$
$$p_1 = \sum_{j=1}^{n} p_{1j}, \quad p_2 = \sum_{j=1}^{n} p_{2j},$$
$$p_3 = \sum_{j=1}^{n} p_{3j}, \quad p_4 = \sum_{j=1}^{n} p_{4j} \tag{8}$$

Normalized Assessment Factor

The value of each assessment factor is normalized over the range of 0–1 to facilitate the efficiency of the overlay analysis in GIS. In the assessment structure, the risk will increase as the following five factors increase: (1) number of geohazards, (2) fault density, (3) fault proximity, (4) population density, and (5) GDP per unit area. These five factors are positive, whereas the other factors are negative. The positive factors are normalized using Eq. (9), and the negative factors are normalized using Eq. (10), as follows:

$$x_{ij} = \frac{x_{ij0} - x_{ij\min}}{x_{ij\max} - x_{ij\min}} \tag{9}$$

$$x_{ij} = \frac{x_{ij\max} - x_{ij0}}{x_{ij\max} - x_{ij\min}} \tag{10}$$

where x_{ij} = normalized value of the factor; x_{ij0} = original value of the factor; and $x_{ij\max}$ and $x_{ij\min}$ = maximum and minimum values of the factors, respectively.

Results and Analysis

Weights of the Assessment Factors

AHP Calibration

According to the assessment structure, the judgment matrix for the index layer can be established first. The judgment matrix should meet the consistency requirement. The AHP weight of each factor in the index layer is calculated using Eq. (4). The consistency ratio, CR, is derived from Eq. (5). The largest eigenvalue ($\lambda_{\max}$) of the judgment matrix is calculated from Eq. (6). The judgment matrix of

Table 2. Weights of the assessment factors from AHP and trapezoidal FAHP methods

Index layer			Subindex layer		
U_i	AHP	Trapezoidal FAHP ($\vec{w}_i$)	U_{ij}	AHP	Trapezoidal FAHP ($\vec{w}_{ij}$)
U_1	0.4434	(0.3772,0.3776,0.3782,0.3794)	U_{11}	0.4977	(0.3818,0.3832,0.3907,0.4009)
			U_{12}	0.2849	(0.3138,0.3173,0.3218,0.3232)
			U_{13}	0.2174	(0.2851,0.2921,0.2936,0.2963)
U_2	0.1692	(0.2412,0.2554,0.2771,0.2847)	U_{21}	0.3244	(0.2777,0.2792,0.2825,0.2848)
			U_{22}	0.3486	(0.2618,0.2716,0.2981,0.3156)
			U_{23}	0.2073	(0.2247,0.2329,0.2457,0.2506)
			U_{24}	0.1197	(0.1818,0.1897,0.2002,0.2028)
U_3	0.3874	(0.3375,0.3456,0.3663,0.3794)	U_{31}	0.4599	(0.3711,0.3739,0.3758,0.3832)
			U_{32}	0.3189	(0.3231,0.3277,0.3359,0.3397)
			U_{33}	0.2211	(0.2864,0.2929,0.2936,0.2965)

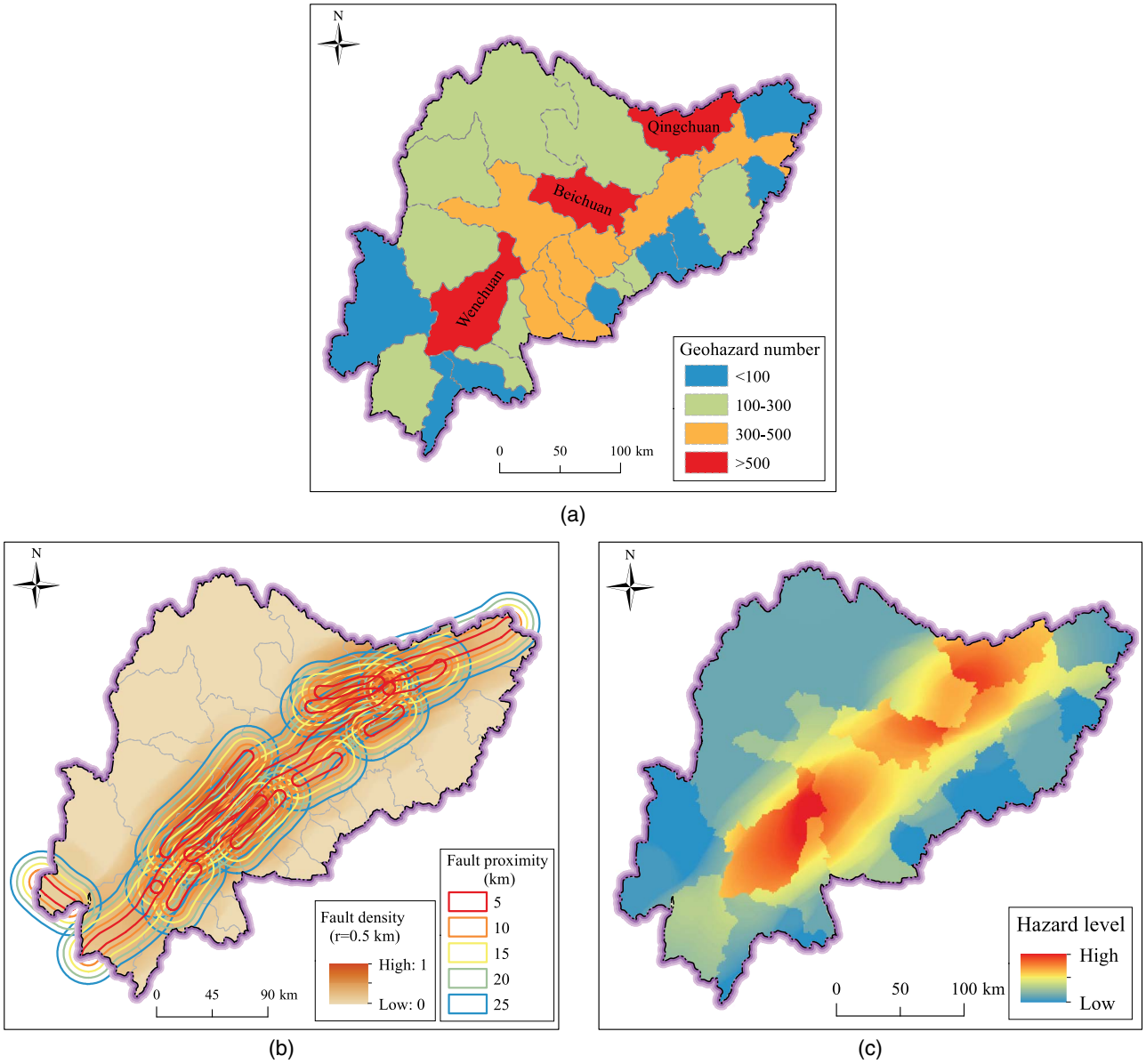

Fig. 4. Spatial distribution of the hazard index: (a) geohazard number; (b) fault density and fault proximity; and (c) hazard levels.

the subindex layer can be similarly established, as well as the weights of the factors in the subindex layer. The judgment matrices of the object, index, and subindex layers are presented in the Supplemental Data section below. Table 2 lists the weights of assessment factors from the AHP method.

Trapezoidal FAHP Calibration

Based on the consistent judgment matrix from the AHP method, the trapezoidal fuzzy number is used to replace the elements in the consistent judgment matrix, and then the fuzzy judgment matrix can be established. Finally, the fuzzy weights with trapezoidal

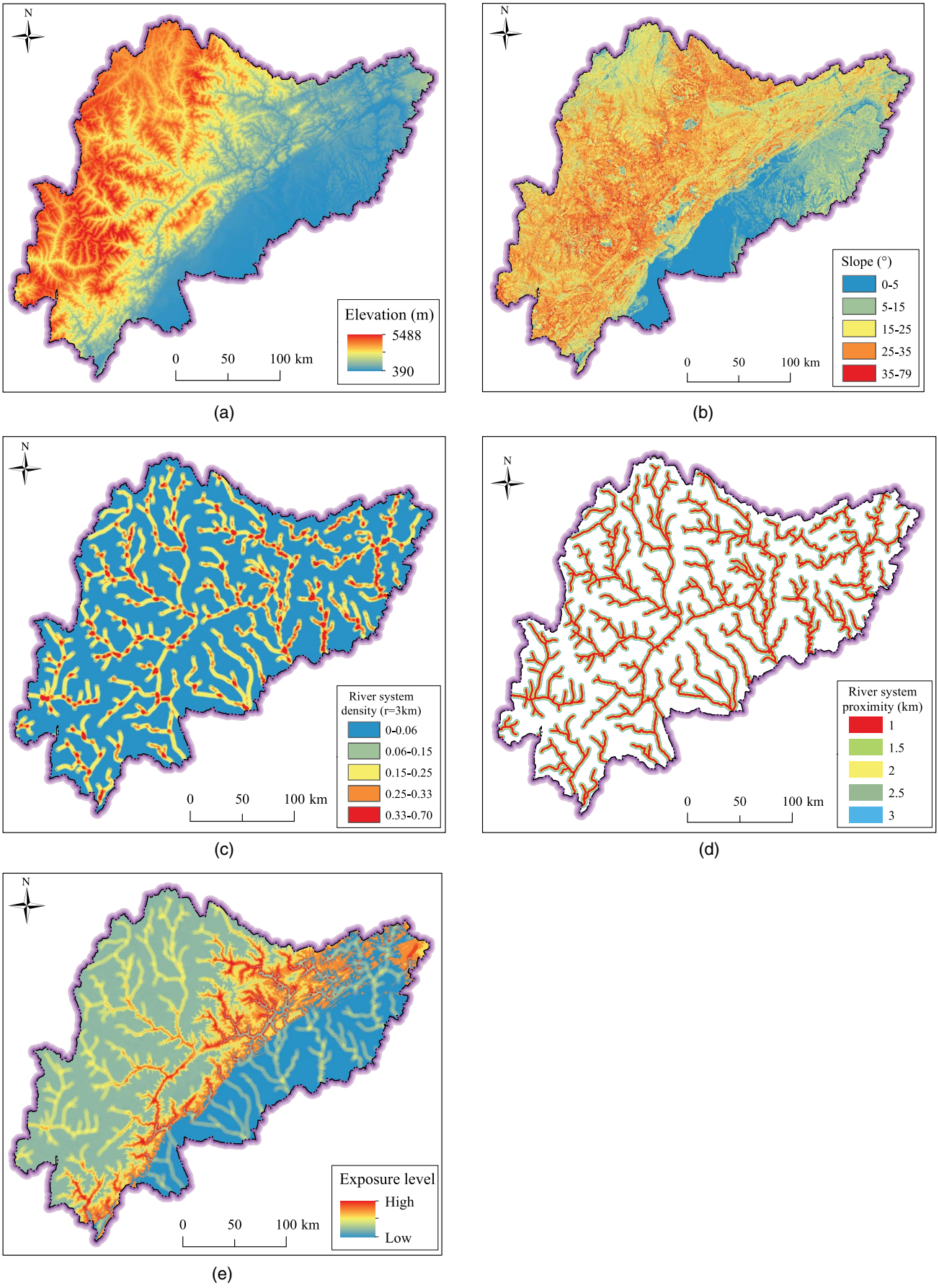

Fig. 5. Spatial distribution of the exposure index: (a) elevation; (b) slope; (c) river system density; (d) river system proximity; and (e) exposure level.

fuzzy numbers can be calibrated using Eqs. (7) and (8). Similarly, the judgment matrix and weights of the subindex layer to the risk can be obtained. The trapezoidal fuzzy judgment matrices are presented in the Supplemental Data section below. Table 2 lists the weights of the assessment factors from the AHP and trapezoidal FAHP methods. The detailed calculation process of the weights can be found in a Lyu et al. (2018a, b).

Analysis

Hazard Level

Based on previous research (Huang 2011; Huang and Li 2014; Fan et al. 2018), information regarding geohazards and faults have been collected. Fig. 4 shows the spatial distribution of the hazard index. Fig. 4(a) shows the geohazard number in different counties. The geohazard number in Wenchuan, Beichuan, and Qingchuan counties is more than 500. Fig. 4(b) shows the spatial distribution of the fault density and fault proximity. The fault density is computed within a circle of radius 0.5 km in GIS. According to Huang and Li (2014), geohazards are distributed within distances of 5, 10, 15, 20, and 25 km from coseismic faults. Therefore, we extracted these ranges using buffer operator analysis in GIS, and the result is shown in Fig. 4(b). After normalizing the assessment factors and applying the weights of each factor listed in Table 2, the raster calculator in GIS is used to compute the different factors. Fig. 4(c) shows the result of the hazard levels. As shown in Fig. 4(c), the area with a high hazard level is located in the region with a dense distribution of faults.

Exposure Level

The exposure index includes topographical features and the local drainage system. Fig. 5 shows the spatial distribution of the exposure index. Figs. 5(a and b) show the topographical features of elevation and slope. According to Huang and Li (2014), 51.4% of geohazards occur in areas within an elevation range of

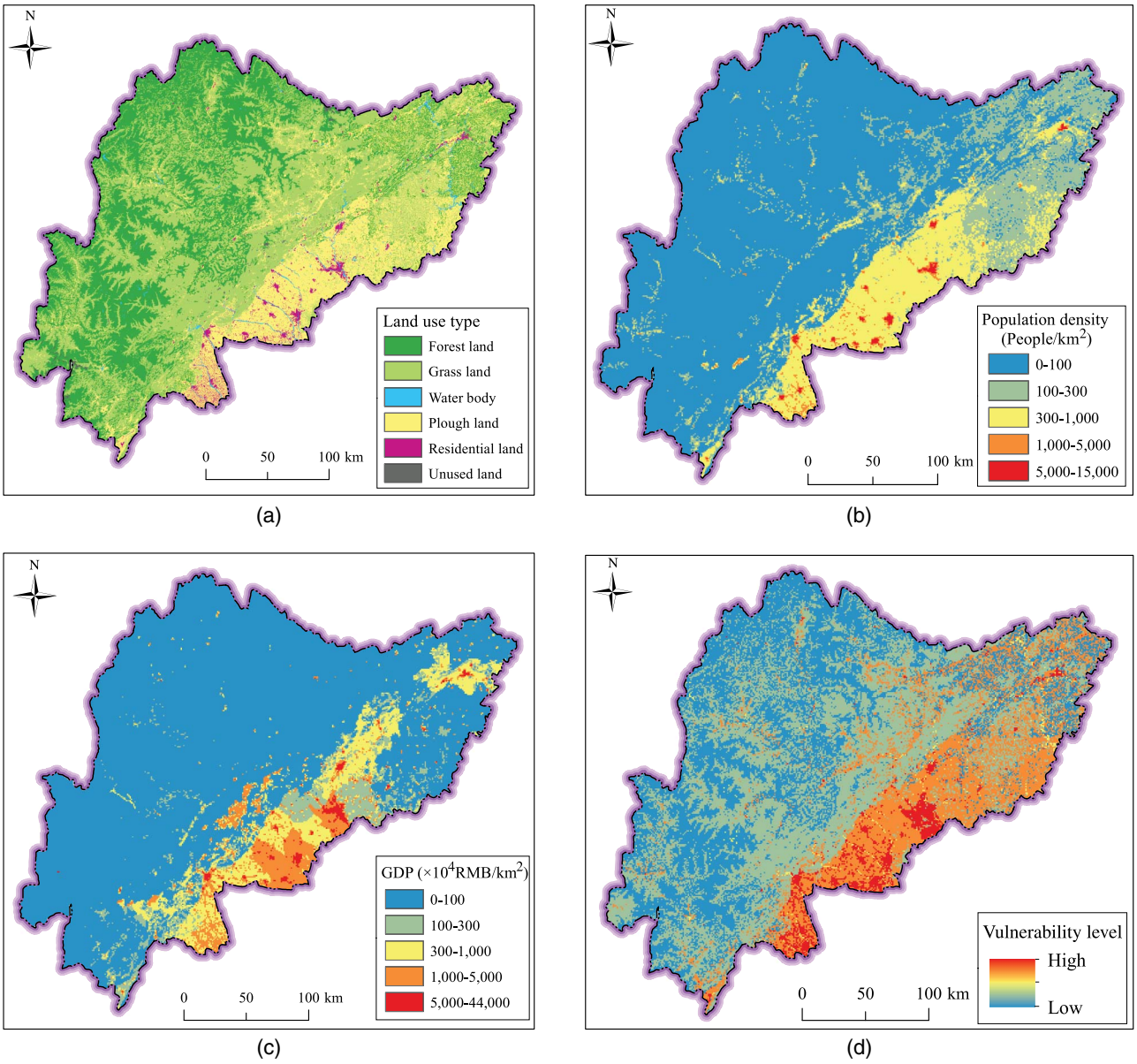

Fig. 6. Spatial distribution of the vulnerability index: (a) land-use type; (b) population density; (c) GDP per unit area; and (d) vulnerability level.

1,000–1,500 m, and 28.6% of geohazards occur in areas within an elevation range of 1,500–2,000 m. Most of the geohazards develop in areas within a slope range of 30°–40°. Based on this investigation, these characteristics were classified into five levels before conducting the overlay analysis. River density and proximity reflect the characteristics of the drainage system (Liu et al. 2016; Lyu et al. 2018a). River density indicates the length of a river channel per unit area, whereas river proximity refers to the distance to the closest river channels. Figs. 5(c and d) show the classification of river density and proximity. According to the scale of the study area, river density was computed within a circle of 3-km radius, whereas the river proximity was 1.0, 1.5, 2.0, 2.5, and 3.0 km in the GIS. These assessment factors were then normalized. The normalized factors combined with their corresponding weights produced the exposure level using a raster calculator in the GIS. Fig. 5(e) shows the spatial distribution of exposure levels. As shown in Fig. 5(e), the highest exposure region is located in the middle zone rather than in regions with high or low elevations.

Vulnerability Level

The vulnerability index includes land-use type, population density, and GDP per unit area. Fig. 6 shows the spatial distribution of the vulnerability index. Resistance to hazards varies among land-use types. Fig. 6(a) shows the different land-use types. Residential land is assessed as having a very high vulnerability level. Therefore, residential land with a high population density may experience catastrophic losses. Conversely, hazards seldom cause damage in either forested or unused land. Thus, their corresponding vulnerability levels are very low. A body of water can discharge rainwater and induce a flash flood. Thus, the vulnerability level of water bodies is classified as medium (Lyu et al. 2019b, 2020). Based on this analysis, the land-use type was reclassified from a risk level of very low to very high before the overlay analysis. Figs. 6(b and c) show the spatial distribution of population density and GDP per unit area. The region with a high population density and high GDP has a high level of vulnerability. Based on our collection of the assessment factors for vulnerability, the vulnerability level can be obtained

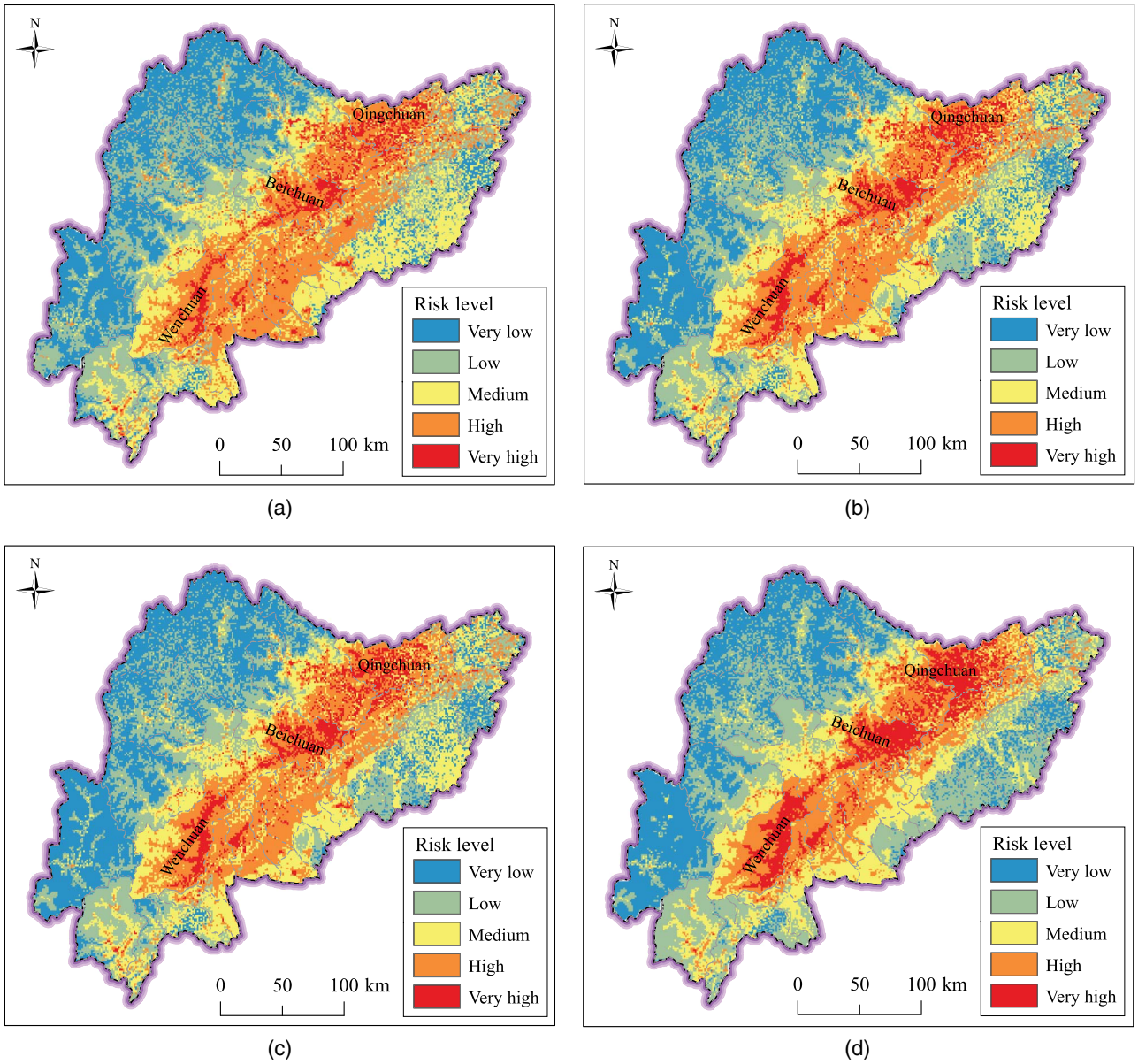

Fig. 7. Assessment results of trapezoidal FAHP: (a) lower bound w_1; (b) left-medium w_2; (c) right-medium w_3; and (d) upper bound w_4.

Nat. Hazards Rev., 2020, 21(3): 05020007

following the normalization process using a raster calculator in the GIS. Fig. 6(d) shows the spatial distribution of vulnerability level. As shown in Fig. 6(d), the vulnerability level is high in the southeast region and low in the northwest region.

Assessment Results for the Trapezoidal FAHP

Based on the risk level of the hazard, exposure, vulnerability indices, and the weights of the different indices, an assessment with fuzzy weights can be constructed. Fig. 7 shows the spatial distribution of the assessment results of the trapezoidal FAHP with fuzzy weights w_1, w_2, w_3, and w_4. As shown in Fig. 7, all four results with lower bound w_1 [Fig. 7(a)], left-medium bound w_2 [Fig. 7(b)], right-medium bound w_3 [Fig. 7(c)], and upper bound w_4 show a similar spatial distribution of risk. Therefore, the very high-risk region would show its risk level exacerbate within the range of fuzzy weights, with an increase from the weights w_1 to w_4. The high-risk region shows a distribution band. The region with a very high-risk level is located in the area adjacent to Wenchuan, Beichuan, and Qingchuan counties. The sector with a high-risk level is distributed throughout the study area. The very low-risk area is located in the northwest, where there are considerable amounts of forest and grasslands.

Discussion

Comparison of Results from AHP and Trapezoidal FAHP

The comparison between the results obtained using AHP and trapezoidal FAHP was used to validate the reasonability of the assessment results. Fig. 8 shows the spatial distribution of the risk level from the original AHP method. As shown in Fig. 8, the AHP assessment result is similar to the trapezoidal FAHP results. It is worth noting that the trapezoidal FAHP can capture areas with high-risk and very high-risk levels more effectively in Wenchuan, Beichuan, and Qingchuan counties, where the geohazard number is more than 500. To compare the differences between the trapezoidal FAHP and the AHP results, the area with different risks can be accounted for using the GIS. Fig. 9 shows a comparison of the regions with varying levels of risk obtained using the trapezoidal FAHP and the AHP. As shown in Fig. 9, the area with a high-risk level from the trapezoidal FAHP is larger than that obtained by the AHP. The sector with a very high-risk level achieved by AHP is located between the range of low bound w_1 and upper bound w_4 using the trapezoidal FAHP. Therefore, the trapezoidal FAHP can provide a broader high-risk assessment result than the AHP method.

Efficiency of Trapezoidal FAHP

To further illustrate the efficiency of the trapezoidal FAHP, the percentages of different risk levels from the original AHP and trapezoidal FAHP were obtained (Fig. 10). The percentage of the very high-risk level from the original AHP is 5.74%, whereas the percentages are 5.42%, 6.32%, 6.42%, and 8.49% from the trapezoidal FAHP. The percentage of the high-risk level is 19.61% from the original AHP, whereas the percentages are 21.16%, 20.73%, 21.09%, and 22.06% from the trapezoidal FAHP. This comparison indicates that the trapezoidal FAHP can capture the regions with high-risk and very high-risk levels better than the original AHP. Further, the trapezoidal FAHP can generate an assessment range, with four choices that managers can consider in decision making. The AHP provides only one assessment result, which may have some biases.

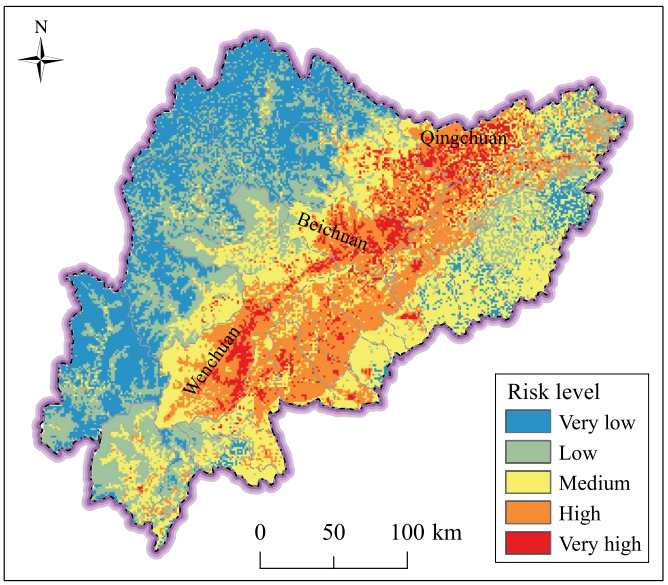

Fig. 8. Risk level of earthquake-triggered geohazards from the original AHP.

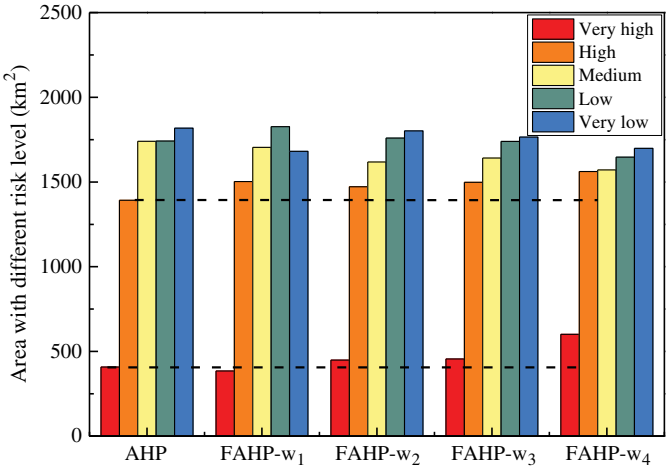

Fig. 9. Comparison of the area with different risk levels between trapezoidal FAHP and AHP.

Conclusions

This study employed both AHP and trapezoidal FAHP methods to assess the risk of earthquake-triggered geohazards surrounding Wenchuan County. Based on the results of this study, the following conclusions are drawn.

1. The trapezoidal FAHP assessment method uses a trapezoidal fuzzy number instead of a crisp number, which overcomes the one-sided deficit of the original AHP method. The trapezoidal fuzzy weights incorporated into the GIS produce a consistent risk assessment result.
2. A comparison of the AHP with the trapezoidal FAHP indicates that the trapezoidal FAHP method captures regions with high-risk and very high-risk levels in the study area. Both the AHP and trapezoidal FAHP results show that the areas with high-risk and very high-risk levels are distributed in the form of a belt along the fault zone. Overall, the risk is high in the southeast and low in the northeast.

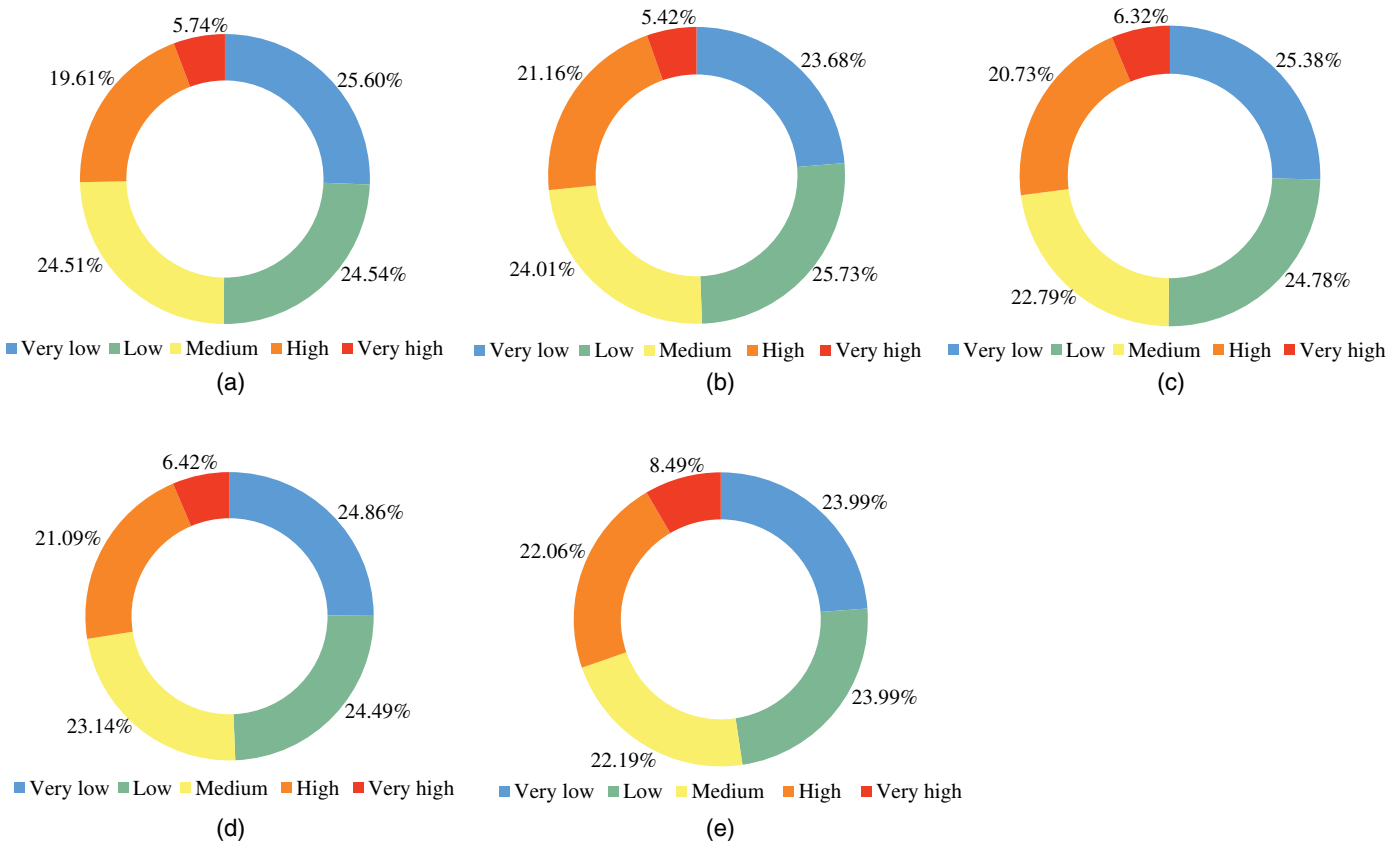

Fig. 10. Percentage of risk levels from the AHP and trapezoidal FAHP methods: (a) original AHP; (b) lower bound FAHP-w_1, (c) left-medium FAHP-w_2; (d) right-medium FAHP-w_3; and (e) upper bound FAHP-w_4.

3. The percentages of high-risk and very high-risk levels obtained from the trapezoidal FAHP are higher than those of the original AHP. The comparison indicates that the trapezoidal FAHP can capture regions with high risk and very high-risk levels. Moreover, the trapezoidal FAHP can produce an assessment range, providing four choices for managers use in decision making, which mitigates the biases that exist in the original AHP.

Data Availability Statement

Data generated or analyzed during the study are available from the corresponding author by request. Information about the Journal's data-sharing policy can be found here: http://ascelibrary.org/doi/10.1061/(ASCE)CO.1943-7862.0001263.

Acknowledgments

The research work described herein was funded by the Research Funding of Shantou University for New Faculty Member (Grant No. NTF19024-2019), and the Innovative Research Funding of the Science and Technology Commission of Shanghai Municipality (Grant No. 18DZ1201102). The sources of financial support are gratefully acknowledged.

Supplemental Data

Tables S1–S4 are available online in the ASCE Library (www.ascelibrary.org).

References

Cheng, C. H., and D. L. Mon. 1994. "Evaluating weapon system by analytical hierarchy process based on fuzzy scales." *Fuzzy Sets Syst.* 63 (1): 1–10. https://doi.org/10.1016/0165-0114(94)90140-6.

Fan, X. M., C. H. Juang, J. Wasowskic, R. Q. Huang, Q. Xu, G. Scaringi, C. J. van Westen, and H. B. Havenith. 2018. "What we have learned from the 2008 Wenchuan earthquake and its aftermath: A decade of research and challenges." *Eng. Geol.* 241 (Jul): 25–32. https://doi.org/10.1016/j.enggeo.2018.05.004.

Gallina, V., S. Torresan, A. Critto, A. Sperotto, T. Glade, and A. Marcomini. 2016. "A review of multi-risk methodologies for natural hazards: Consequences and challenges for a climate change impact assessment." *J. Environ. Manage.* 168 (Mar): 123–132. https://doi.org/10.1016/j.jenvman.2015.11.011.

GDC (Geospatial Data Cloud). 2018. "Topographic data." Accessed April 20, 2018. http://www.gscloud.cn/.

Godschalk, D. R. 2003. "Urban hazard mitigation: Creating resilient cities." *Nat. Hazards Rev.* 4 (3): 136–143. https://doi.org/10.1061/(ASCE)1527-6988(2003)4:3(136).

Huang, R. Q. 2011. "After effect of geohazards induced by the Wenchuan earthquake." *J. Eng. Geol.* 19 (2): 145–151.

Huang, R. Q., and W. L. Li. 2014. "Post-earthquake land-sliding and long-term impacts in the Wenchuan earthquake area, China." *Eng. Geol.* 182 (Nov): 111–120. https://doi.org/10.1016/j.enggeo.2014.07.008.

Jalayer, F., R. De Risi, M. Giugni, G. Manfredi, P. Gasparini, and G. Cavan. 2014. "Probabilistic GIS-based method for delineation of urban flooding risk hotspots." *Nat. Hazards* 73 (2): 975–1001. https://doi.org/10.1007/s11069-014-1119-2.

Kamal, H. A., B. M. Ayyub, and W. A. Abdullah. 2013. "Land subsidence in arid terrain: Methodology toward risk analysis." *Nat. Hazards Rev.* 14 (4): 268–280. https://doi.org/10.1061/(ASCE)NH.1527-6996.0000099.

Laarhoven, P. J. M. V., and W. Pedrycz. 1983. "A fuzzy extension of Saaty's priority theory." *Fuzzy Sets Syst.* 11 (1–3): 199–227. https://doi.org/10.1016/S0165-0114(83)80082-7.

Liu, R., Y. Chen, J. Wu, L. Gao, D. Barrett, T. Xu, and J. Yu. 2016. "Assessing spatial likelihood of flooding hazard using naïve Bayes and GIS: A case study in Bowen Basin, Australia." *Stoch. Environ. Res. Risk Assess.* 30 (6): 1575–1590. https://doi.org/10.1007/s00477-015-1198-y.

Lu, Y., and J. P. Xu. 2015. "Comparative study on the key issues of post-earthquake recovery and reconstruction planning: Lessons from the United States, Japan, Iran, and China." *Nat. Hazards Rev.* 16 (3): 04014033. https://doi.org/10.1061/(ASCE)NH.1527-6996.0000172.

Lyu, H. M., J. S. Shen, and A. Arulrajah. 2018a. "Assessment of geohazards and preventative countermeasures using AHP incorporated with GIS in Lanzhou, China." *Sustainability* 10 (2): 304. https://doi.org/10.3390/su10020304.

Lyu, H. M., S. L. Shen, A. N. Zhou, and J. Yang. Forthcoming. "Risk assessment of mega-city infrastructures related to land subsidence using improved trapezoidal FAHP." *Sci. Total Environ*. https://doi.org/10.1016/j.scitotenv.2019.135310.

Lyu, H. M., S. L. Shen, A. N. Zhou, and J. Yang. 2019a. "Perspectives for flood risk assessment and management for mega-city metro system." *Tunn. Undergr. Sp. Tech.* 84 (Feb): 31–44. https://doi.org/10.1016/j.tust.2018.10.019.

Lyu, H. M., S. L. Shen, A. N. Zhou, and W. H. Zhou. 2019b. "Flood risk assessment of metro systems in a subsiding environment using the interval FAHP-FCA approach." *Sustain. Cities Soc.* 50 (Oct): 101682. https://doi.org/10.1016/j.scs.2019.101682.

Lyu, H. M., W. J. Sun, S. L. Shen, and A. Arulrajah. 2018b. "Flood risk assessment in metro systems of mega-cities using a GIS-based modeling approach." *Sci. Total Environ.* 626 (Jun): 1012–1025. https://doi.org/10.1016/j.scitotenv.2018.01.138.

Lyu, H. M., W. J. Sun, S. L. Shen, and A. N. Zhou. 2020. "Risk assessment using a new consulting process in fuzzy AHP." *J. Constr. Eng. Manage.* 146 (3): 04019112. https://doi.org/10.1061/(ASCE)CO.1943-7862.0001757.

Qi, S., Q. Xu, H. Lan, B. Zhang, and J. Liu. 2010. "Spatial distribution analysis of landslides triggered by 2008.5.12 Wenchuan earthquake, China." *Eng. Geol.* 116 (1): 95–108. https://doi.org/10.1016/j.enggeo.2010.07.011.

REDCP (Resource and Environment Data Cloud Platform). 2018. "Gross domestic product data." Accessed April 30, 2018. http://www.resdc.cn/.

Saaty, T. L. 1977. "A scaling method for priorities in hierarchical structures." *J. Math. Psychol.* 15 (3): 234–281. https://doi.org/10.1016/0022-2496(77)90033-5.

Saaty, T. L. 2008. "Decision making with the analytic hierarchy process." *Int. J. Serv. Sci.* 1 (1): 83–98. https://doi.org/10.1504/IJSSCI.2008.017590.

Saaty, T. L. 2010. *Creative thinking, problem solving and decision making.* 3rd ed. Pittsburgh, PA: RWS Publications.

Wang, G. H., R. Q. Huang, S. D. N. Lourenço, and T. Kamai. 2014. "A large landslide triggered by the 2008 Wenchuan (M8.0) earthquake in Donghekou area: Phenomena and mechanisms." *Eng. Geol.* 182 (Nov): 148–157. https://doi.org/10.1016/j.enggeo.2014.07.013.

Xu, C., X. W. Xu, X. Yao, and F. C. Dai. 2014. "Three (nearly) complete inventories of landslides triggered by the May 12, 2008 Wenchuan Mw 7.9 earthquake of China and their spatial distribution statistical analysis." *Landslides* 11 (3): 441–461. https://doi.org/10.1007/s10346-013-0404-6.

Yao, X., and L. J. Li. 2016. "Spatial-temporal assessment of debris flow risk in the Ms 8.0 Wenchuan Earthquake-disturbed area." *J. Disaster Res.* 11 (4): 720–731. https://doi.org/10.20965/jdr.2016.p0720.

Yin, Y., F. Wang, and P. Sun. 2009. "Landslide hazards triggered by the 2008 Wenchuan earthquake, Sichuan, China." *Landslides* 6 (2): 139–152. https://doi.org/10.1007/s10346-009-0148-5.

Zhang, D. X., and G. H. Wang. 2007. "Study of the 1920 Haiyuan earthquake-induced landslides in Loess (China)." *Eng. Geol.* 94 (1): 76–88. https://doi.org/10.1016/j.enggeo.2007.07.007.

Zhang, H. F. 2016. "Household vulnerability and economic status during disaster recovery and its determinants: A case study after the Wenchuan earthquake." *Nat. Hazards* 83 (3): 1505–1526. https://doi.org/10.1007/s11069-016-2373-2.

Zhang, J., H. Z. Chen, H. W. Huang, and Z. Luo. 2015. "Efficient response surface method for practical geotechnical reliability analysis." *Comput. Geotech.* 69 (Sep): 496–505. https://doi.org/10.1016/j.compgeo.2015.06.010.

Zhang, J., H. Wang, H. W. Huang, and L. H. Chen. 2017. "System reliability analysis of soil slopes stabilized with piles." *Eng. Geol.* 229 (7): 45–52. https://doi.org/10.1016/j.enggeo.2017.09.009.

Zhou, W., C. Tang, T. W. J. Van Asch, and M. Chang. 2016. "A rapid method to identify the potential of debris flow development induced by rainfall in the catchments of the Wenchuan earthquake area." *Landslides* 13 (5): 1243–1259. https://doi.org/10.1007/s10346-015-0631-0.